2020 Spring Technical Meeting
Central States Section of The Combustion Institute
May 17–19, 2020
Huntsville, Alabama

# Optical Investigation of Catalyst Heating Operation in a Light-Duty Compression-Ignition Engine

*Srinath Subramanian[1,*], David A. Rothamer[1]*

*[1]Dept. of Mechanical Engineering, UW-Madison, Madison, United States*
*[*]Corresponding Author Email: ssubramani24@wisc.edu*

**Abstract:** It is well known that cold start engine operation contributes a majority of tail-pipe emissions during a vehicle drive cycle. Aftertreatment catalysts have poor conversion efficiency during this period due to low conversion efficiency at temperatures less than their light-off temperature. A late post injection strategy, with a delayed injection to increase exhaust enthalpy, can help decrease the time required to heat-up the catalyst. However, late injections into conditions with decreasing temperature and density can result in high emissions and combustion instability. In this study a three-injection strategy with a late-post injection was investigated in an optically-accessible engine. For the first two injections (pilot and main) timing and duration were held constant as the post injection timing was swept and duration varied to hold load constant, at a relevant light-load catalyst heating operating condition. Simultaneous double-pass schlieren and OH chemiluminescence data were acquired in an optically-accessible 0.4 L single-cylinder engine to understand spray characteristics and combustion behavior for #2 diesel fuel. Optical images analysis revealed higher liquid penetration and lower vaporization of the liquid fuel jet as post injection is retarded. It is also observed that retarding post injection timing to +25 CAD resulted in lower observed soot concentration in the piston bowl.

***Keywords: Catalyst heating operation, post injection, emissions, optical engine, spray***

## 1. Introduction

It is projected that about 74% of the total energy consumed by the transportation sector in 2050 may still be expected to come from fossil fuel-based resources [1]. This prompts an urgent need to reduce criteria pollutants and $CO_2$ emissions from these sources. Studies indicate that the cold-start phase of engine operation is responsible for approximately 90% of volatile organic compound (VOC) emissions and 30% of nitrogen oxide (NOx) emissions [2]. Rapidly reaching temperatures for optimal performance of aftertreatment devices designed to control engine-out criteria pollutants is critical for reducing emissions during cold-start operation.

### *1.1. Diesel spray*

A brief overview of the physical process involved during compression-ignition of diesel-like fuels is provided here as a reference to readers. Liquid fuel injected at high pressure into the combustion

chamber entrains ambient gases which vaporize the fuel droplets and heat the fuel jet up to kinetically-relevant temperatures. Low-temperature ignition occurs first in the lean periphery of the jet followed by low-temperature and then high-temperature ignition in rich regions of the jet establishing mixing-controlled combustion. A more detailed description of the diesel spray development and ignition process can be found here [3–5]. The liquid length of the spray, defined as the maximum axial penetration of liquid phase fuel, is an important parameter that can strongly impact engine-out hydrocarbon (HC) emissions if liquid impingement takes place. Liquid length is inversely corelated to ambient temperature and density [6]. Making ambient conditions during injection an important parameter influencing liquid penetration and combustion characteristics of high-pressure fuel sprays.

*1.2. Aftertreatment components and characteristics*

Modern diesel engine aftertreatment systems consist of a diesel oxidation catalyst (DOC), a diesel particulate filter (DPF), and a selective catalytic reduction (SCR) system. The efficacy of these devices in converting criteria emissions to less harmful gases is highly temperature dependent [7–9]. Recent work using an integrated DPF with downsized SCR demonstrated reduction in threshold temperature for urea dosing to 180 °C [10]. Dosing SCR with urea at temperatures lower than the threshold limit can lead to formation of solid deposits [11]. Similarly, DOCs, responsible for hydrocarbon (HC) oxidation, are characterized with a light-off temperature in the range of 200-250 °C [9]. Particulate matter (PM) build-up can significantly increase the pressure drop across the DPF which then requires regeneration to burn off built up PM to restore the pressure drop to normal operating levels. The temperature sensitive operation of these devices highlights the need for an effective aftertreatment thermal management strategy, which can ensure rapid heat-up while maintaining low emissions during the heat-up period.

*1.3. Thermal management techniques*

Active thermal management of aftertreatment devices has been a topic of continuous research and has gained significant traction with tightening regulations. Targeted electric heating of aftertreatment components during cold start phase has been previously investigated [12,13], this method however requires significant hardware modification and a dedicated control strategy. Cylinder deactivation [14] can be employed, but this also requires significant hardware modifications. On the other hand, in-cylinder strategies, such as using combustion of a late post injection during the expansion stroke [9,14,15], require no hardware modification in a modern engine control environment. The objective of this study is to investigate late injections in the expansion stroke for heating of the exhaust aftertreatment system.

For late injection operation strategies at least three injections are employed during the cycle: a pilot injection, a main injection, and a post injection. The role of each injection can be summarized as following:

- The pilot injection (first injection) is used to control the start of the heat release and, therefore, the combustion noise.
- The main injection (second injection) is phased close to top dead center (TDC) and provides a significant amount of the work output, i.e., load (gross indicated mean effective pressure (GIMEP)), and helps to insure stable ignition and combustion of the post injection.
- The post injection (third injection) is used to increase the exhaust gas temperature and enthalpy and to provide the remaining work for the desired engine load.

Effectiveness of post injection in maintaining aftertreatment catalyst temperatures has been previously demonstrated by Parks et. al [14]. Retarding post injection timing late into the expansion stroke can allow reduced work extraction, resulting in increased exhaust enthalpy. However, in-cylinder conditions for post injection represent a significant challenge for stable ignition and combustion as the in-cylinder temperature and in-cylinder density are decreasing for late injection times. These conditions, coupled with low oxygen concentration, can result in wall wetting and incomplete combustion of the fuel causing increased HC and carbon monoxide (CO) emissions. For cold start conditions this results in increased emissions as the aftertreatment system has not reached temperatures to efficiently convert these species to $CO_2$ and $H_2O$.

Previous optical investigation of post injections in diesel engines has been largely focused on evaluating effectiveness of post injections in reducing HC and soot engine-out emissions [16–18]. In a non-engine study performed in a constant volume combustion chamber, Genzale et al. [19] investigated spray penetration at very low densities (1.2 to 3.0 kg/m$^3$) and relatively high ambient temperatures (800-1400 K). The focus in this study was on very late post injections where the fuel is not intended to burn significantly in-cylinder and the objective was to understand the propensity for cylinder liner impingement and oil dilution. They observed an increasing liquid length extending up to vessel boundary as ambient density and temperature decreased. These are not the conditions of interest in the current work where combustion of the fuel in-cylinder is desired.

Due to the limited optical studies in engines focused on the spray and combustion behavior of post injections intended for catalyst heating operation prior to light of the DOC, the current work focuses on these conditions. The work visualizes the post injection combustion process in an optical engine using simultaneous high-speed schlieren and OH chemiluminescence imaging. Schlieren image data show density gradients in-cylinder allowing for visualization of the fuel jet penetration and mixing, as well as, identification of areas of fuel liquid, fuel vapor, and soot. Imaging of the OH chemiluminescence from the OH* radical can be used to identify regions of ongoing high-temperature combustion [20]. The main objective of current work is to visualize late post injections and their subsequent combustion to better understand factors that may influence emissions formation and combustion instability at late post-injection times relevant to catalyst heating operation. With this improved understanding, adjustments to fuel properties or engine operation and design may be feasible to improve operation at these conditions.

## 2. Methods

Experiments for this study were performed with 2007 certification ultra-low sulfur diesel (Haltermann Solutions). Basic fuel property information is listed in Table 1. A production 7-hole common-rail diesel injector (Bosch CRIP2 MI) with an orifice diameter of 141 µm and an included angle of 144˚was used for fuel injection.

Table 1: Certification low-sulfur diesel properties

| Fuel Property | Units | Value |
|---|---|---|
| Cetane Number | - | 45.6 |
| Lower Heating Value | MJ/kg | 42.62 |
| Density | kg/m$^3$ | 855 |
| Viscosity (at 40°C) | cSt | 2.4 |
| H/C ratio | - | 1.84:1 |

The major characteristics of the optically accessible engine used are listed in Table 2, and a schematic diagram detailing the engine's construction is provided in Figure 1. The core of the optical engine is a Bowditch extended piston with a piston cap containing a 29-mm thick UV-grade fused silica window, providing a 53.3 mm diameter field of view (FOV) into the combustion chamber. The 7-hole DI injector is centrally located, i.e., its axis is aligned with the cylinder axis. The cylinder head has a two-valve design one each for intake and exhaust gases. In-cylinder pressure data were collected at a resolution of 0.25 crank angle degrees (CAD) using a piezoelectric in-cylinder pressure transducer (Kistler, model 6053BB60) connected to a charge amplifier (Kistler, model 5010). Crank angles are listed as negative for values before TDC compression (-360 to 0) and positive for values after TDC of compression (0 to +360). Data acquisition was timed to the engine using an optical shaft encoder (BEI, model H25). Intake air mass flow was controlled and measured using calibrated choked-flow orifices. Orifice upstream pressure was controlled to maintain the desired mass flow rate. Intake temperature was controlled using an in-line process air heater (Hotwatt, AH1201 2.8-kW). The surfaces of the intake system downstream of the inline heater were heated and insulated to maintain the intake temperature.

Table 2: Engine geometry details.

| Parameter | Units | Value |
|---|---|---|
| Bore | mm | 82 |
| Stroke | mm | 76.2 |
| Displacement | $cm^3$ | 402 |
| Compression Ratio | - | 14.0:1 |
| IVC/IVO | CAD | -164˚/347˚ |
| EVO/EVC | CAD | 164˚/375˚ |
| Skip-Fire Ratio | - | 10:1 |

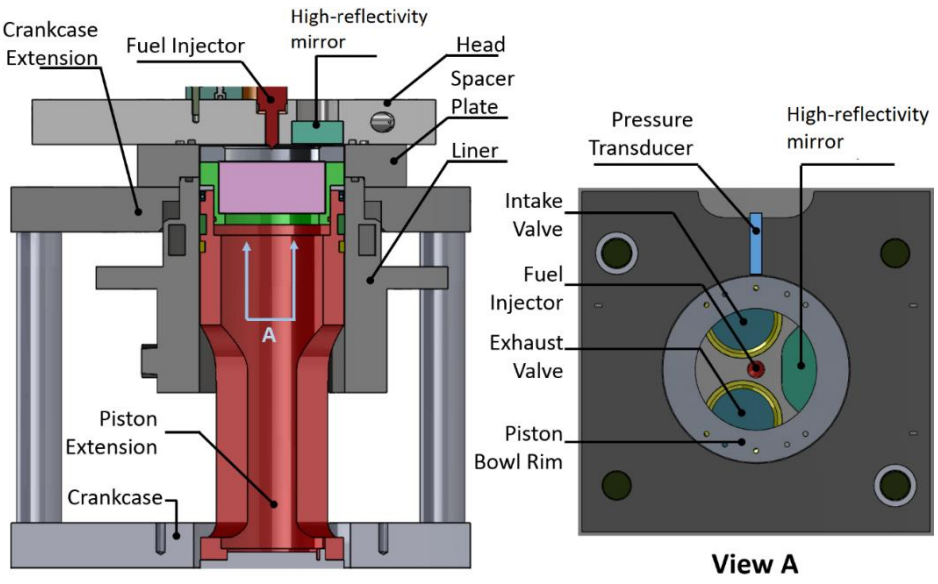


Figure 1: Schematic diagram of the optically accessible engine indicating the major features of the combustion chamber (reproduced with permission from [21])

A brief description of imaging setup and hardware used for schlieren and OH chemiluminescence imaging is provided here, a more detailed description of the setup can be found in [21,22]. OH chemiluminescence images were collected at a frame rate of 40 kHz with an exposure duration of 20 μs, using a high-speed camera (Vision Research, model Phantom v7.1) which has a lens-coupled image intensifier (Night Vision Systems, model 2071). The high-speed camera had a 310-nm wavelength bandpass filter (Asahi Spectra, model XBPA310, 10-nm FWHM) with a f/4.5 105-mm UV lens (Nikon, UV-Nikkor) mounted on it. A single blue (460-nm center wavelength) LED (Luminus, model CBT-120) operated at a drive current of 11 A was used as an illumination source for schlieren imaging. A precision-ground stainless steel mirror installed in the engine head was cleaned after each run (10 fired cycles) to ensure that the surface was free from fuel and soot residue. Schlieren images were captured using a high-speed camera (Vision Research, model Phantom v1840) at a frame rate 80 kHz with a 210-ns exposure duration using a f/4 200-mm lens (Nikon, Nikkor).

*2.2. Operating conditions*

Operating conditions for this study were derived from recent work by Ross et. al [23]. They investigated HC emissions during catalyst heating operation in a multi-cylinder engine setup for two different fuels of similar reactivity but different volatility. A similar injection strategy, where the pilot and main injection timing and duration are held constant as post injection timing is swept is adopted for this work. Important operating parameters are listed in Table 3, the optical engine was operated at a slightly reduced speed of 1200 revolutions per minute (RPM). Skip-fired operation and lab setup restricted use of any exhaust gas recirculation (EGR) during these experiments. Results for three start-of-injection times for the post injection are discussed here, out of a wider post start of injection command (SOI) timing sweep. All SOIs listed in the paper correspond to the commanded SOI and a short delay exists (~300 μs) between the commanded SOI and the start of fuel flow in-cylinder. The SOI times and commanded duration of injection (DOI) in milliseconds for post-injection cases are listed in Table 4. These three conditions are referred to as Post SOI 15, Post SOI 19 and Post SOI 25 throughout. Care was taken to match boundary conditions as closely as possible between conditions.

Table 3: Operating and boundary conditions.

| **Parameter** | **Units** | **Value** |
|---|---|---|
| Speed | RPM | 1200 |
| EGR | % | 0 |
| Intake Temperature | °C | 55 |
| Intake Pressure | kPa | 152 |
| Injection Pressure | MPa | 50 |
| Pilot SOI | CAD | -17 |
| Pilot DOI | ms | 0.41 |
| Main SOI | CAD | 1 |
| Main DOI | ms | 0.43 |
| Coolant & Oil Temperature | °C | 50 |

Table 4: Post injection timing and duration.

| Post SOI [CAD] | Post DOI [ms] |
|---|---|
| 15 | 0.58 |
| 19 | 0.86 |
| 25 | 0.86 |

## 3. Results and Discussion

### *3.1. Pressure and heat release*

Figure 2 (a) compares, pressure and apparent heat release rate (AHRR) from optical engine experiments and metal engine data from [23] for Post SOI 15. AHRR is calculated from filtered pressure trace using a first law balance. Each injection event is marked by its own ignition event which are captured in the pressure and AHRR plots. Combustion phasing and AHRR features like magnitude of peak heat release rate for the post injection and burn duration associated with all three injections are reasonably, but not perfectly, matched between the engines. This enables some comparison of results to those in [23]. However, there are significant differences between the two studies as well. These include differences in EGR rate (0% for the optical engine vs. 30% for the metal engine), higher pressure and temperature during the expansion stroke in the optical engine, differences in-cylinder geometry and flow, and differences in in-cylinder surface temperatures. Because of these differences, a direct comparison between results in optical and metal engines is not possible, instead, the optical results are used here to develop understanding of the general physics and processes occurring during late post injections and the metal engine results from the previous study are used as a reference for the impacts on engine emissions that these may have.

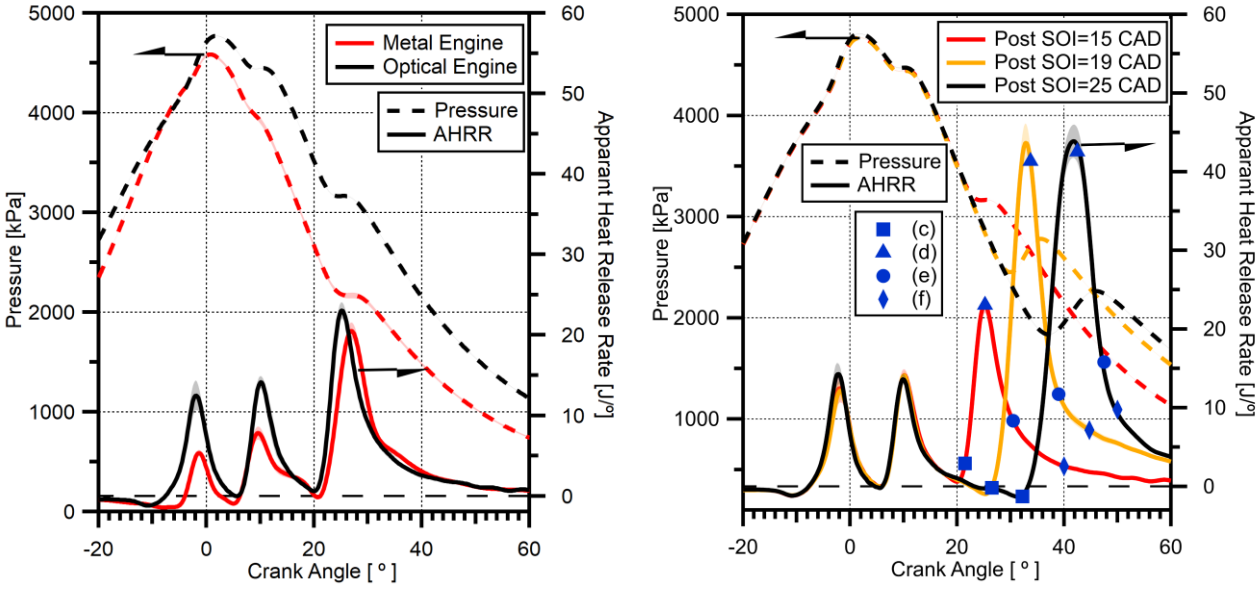


(a) (b)

Figure 2: (a) Pressure and heat release comparison between optical and metal engine ([23]) for Post SOI 15. (b) Pressure and heat release for the three post injection SOI times in the optical engine. Markers represent relative crank angle position of images (c), (d), (e) and (f) in Figure 5, 6, and 7. Shaded bands represent one standard deviation about mean.

Figure 2 (b) shows pressure and AHRR data for all three conditions from optical engine experiments at the operating conditions specified in Table 3. As observed before in Figure 2 (a) three separate combustion events occur each followed by increase in in-cylinder pressure. Overall heat release associated with pilot and main injection are consistently matched between conditions within the experimental variability. Ensuring little or no variation in-cylinder conditions between each condition before the introduction of the post injection. As the post injection timing is delayed, lower ambient temperature and pressure at the time of injection results in increased ignition delay and for the Post SOI 19 and 25 cases. Longer injection duration for these cases also results in higher peak heat release rates and overall heat release. Figure 2 (b) also has markers placed on the AHRR curves for each condition to represent crank angle location of in-cylinder images which are discussed in the following section.

*3.2. Pilot and main injections*

Schlieren images for the pilot injection are shown in Figure 3 for different times after SOI. The images in Figure 3, and the figures which follow, focus on a single fuel jet issuing from the 7-hole injector. The origin in the images corresponds to the center of the fuel injector. The fuel jet of interest issues forth from the fuel injector directed vertically in the images. At the top edge of the images a dark curved boundary is present which corresponds to the edge of the piston bowl.

Figure 3 (a) shows the in-cylinder density gradients present due to temperature difference in the in-cylinder gases before any fuel is introduced. The dark semicircle at the bottom of the image is due to the fuel injector tip. The horizontal black region is a boundary between the polished cylinder head surface and the high reflectivity mirror inserted in the cylinder head. Figure 3 (b), (c), and (d) show the development of the pilot jet at different crank angles during the pilot injection. Liquid fuel which results in lower signals (darker regions) than vaporized fuel, can be clearly distinguished from the background in Figure 3 (b) and (c). As the jet propagates and entrains the ambient air in-cylinder the liquid fuel begins to vaporize. The image in Figure 3 (d) is slightly after the end of injection where air entrainment has resulted in vaporization of most of the fuel.

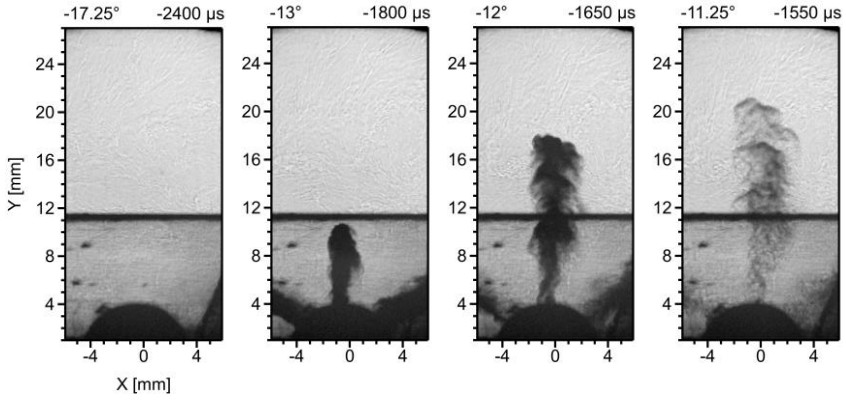


Figure 3: (a) Schlieren background, (b) & (c) pilot jet development 1 and 2 CAD after SOI, (d) pilot jet mixing 3 CAD after SOI. Images are labeled with crank angle and time in microseconds relative to TDC they were acquired at.

Shortly after the end of injection, the pilot fuel injected ignites and the heat release and temperature variations associated with combustion result in significant gradients in density and, therefore,

schlieren signal in-cylinder. This is seen in the first image of the main injection sequence shown in Figure 4, where the main injection propagates into a much more variable background schlieren signal than is seen prior to any injection in Figure 3 (a). Even with this greater background schlieren signal variation the main injection is clearly visible in Figure 4 (a) and (b). Figure 4 (b) shows the main injection right after the end of injection around the time of ignition. The next image time is after ignition for the main injection (Figure 4 (c)). After ignition the area where the main injection jet was becomes suddenly darker in Figure 4 (c) and (d) a result of light extinction caused by soot formation.

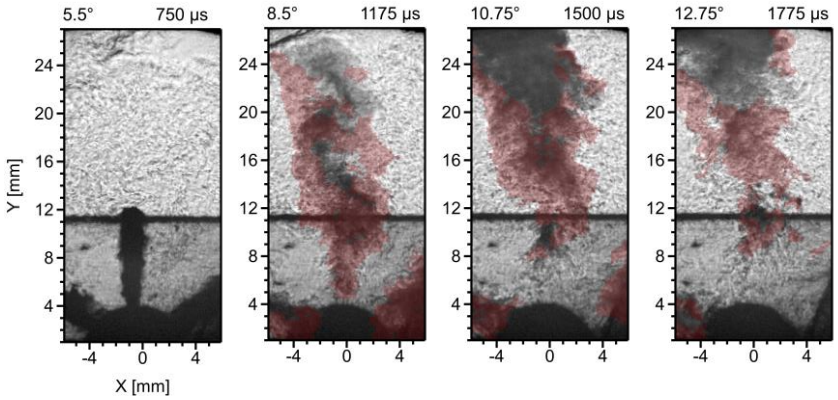


(a) (b) (c) (d)

Figure 4: Schlieren images of main injection developing at crank angles indicated in the figures. OH* signal overlaid in transparent red.

*3.3. Post injection*

Figure 5, Figure 6, and Figure 7 track the development of the post injection jet and combustion for post injection SOIs of 15, 19, and 25 CAD, respectively. The first set of 2 images, (a) and (b), in all three figures capture the spray 2.25 and 3.25 CAD after SOI. The schlieren images at these two times depict the penetrating jet. For Post SOI 15 and 19 some degree of vaporization is seen in the head of the jet, however, for Post SOI 25 little vaporization of the liquid fuel is indicated in this region. As the post injection is retarded the density and temperature of the in-cylinder gases at the SOI for the post injection are reduced. This results in reduced entrainment of in-cylinder gases and simultaneously lower temperatures for the gases that are entrained, causing reduced vaporization and longer liquid lengths for later post injection times. The liquid for the Post SOI 25 case appears to extend almost all the way to the piston bowl wall, such long liquid lengths can result in piston bowl and cylinder liner wetting which can impact engine-out HC emissions.

In the same figures, images (c), (d), (e) and (f) show the schlieren images overlaid with OH signal, shown in transparent red, to track regions of OH* formation and hence heat release. After a short ignition delay, high temperature reactions and heat released are indicated at the periphery of the jets as shown in image (c), at the approximate time of start of combustion (SOC), for all three post injection times. The region of the jet corresponding to this early stage heat release is consistent with simulation results by Kim et al. [4].

Image set (d) in all three figures, occurs after the end of injection at the crank angle position corresponding to the highest AHRR. For all three post injection times, a significant dark region is seen in the schlieren imaging in the upper half of the images near the piston bowl wall,

hypothesized to be the result of high soot concentrations and soot extinction in this region. OH* emission is present in a number of regions starting near the injector and surrounding the region of high soot concentration. The targeting of the post injection jet is significantly different for the three post injection times, as shown in Figure 8. For the late injection cases, the fuel jet penetrates beyond the piston bowl wall (corresponding to the upper edge of the field of view). This may explain the lower apparent soot light extinction seen for the Post SOI 25 case in image (d) relative to the Post SOI 15 and 19 cases.

Images (e) and (f) represent the late oxidation phase captured approximately 5 CAD after peak HRR and 25 CAD after SOI, respectively. Oxidation of unburnt fuel and soot is clearly ongoing as indicated by OH* emission even at these late image times. Soot concentrations are still relatively high in the piston bowl region with very high concentration indicated by the strong extinction for Post SOI 19. Higher soot concentrations may be present outside of the field of view closer to the cylinder liner for Post SOI 25 due to the jet targeting, but this region is outside the current field of view for the measurements.

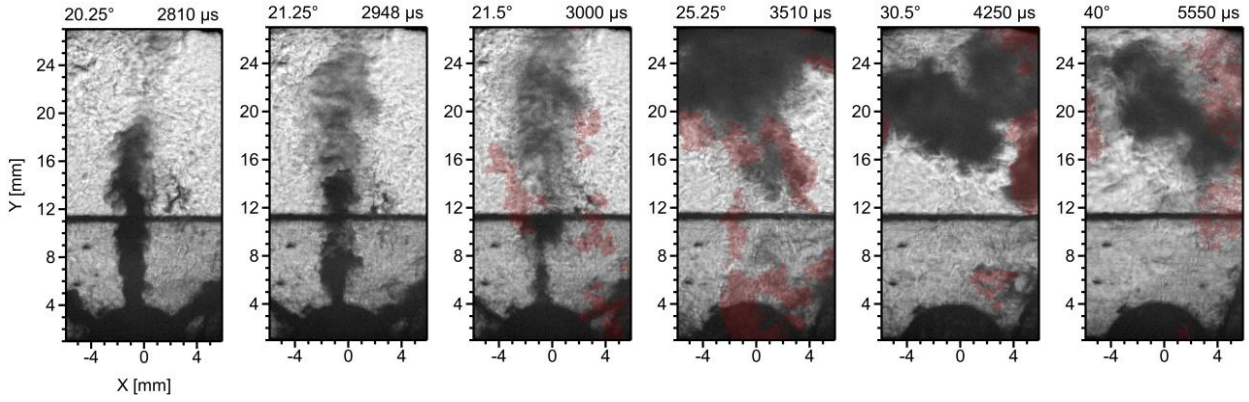


Figure 5: Post SOI=15 CAD: OH* signal overlaid in transparent red. Fuel jet (a) 2.25 CAD and (b) 3.25 CAD after SOI; (c) SOC; (d) location of peak AHRR; (e) and (f) late soot oxidation.

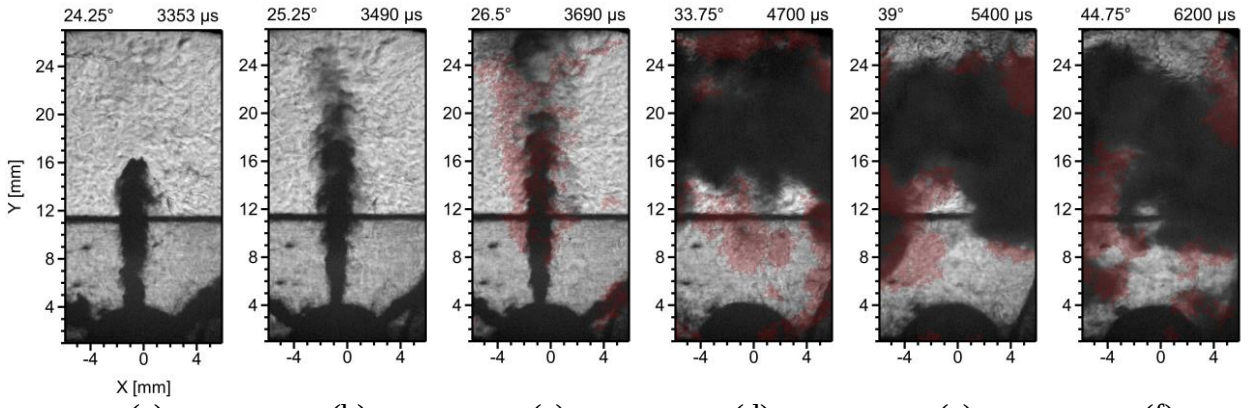


Figure 6: Post SOI=19 CAD: OH* signal overlaid in transparent red. Fuel jet (a) 2.25 CAD and (b) 3.25 CAD after SOI; (c) SOC; (d) time of peak AHRR; (e) and (f) late soot oxidation.

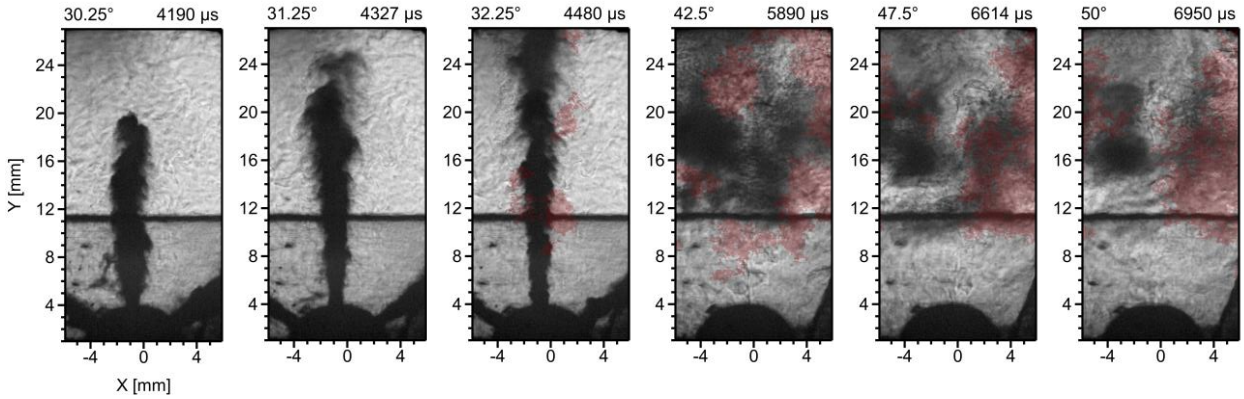


Figure 7: Post SOI=25 CAD: OH* signal overlaid in transparent red. Fuel jet (a) 2.25 CAD and (b) 3.25 CAD after SOI; (c) SOC; (d) time of peak AHRR; (e) and (f) late soot oxidation.

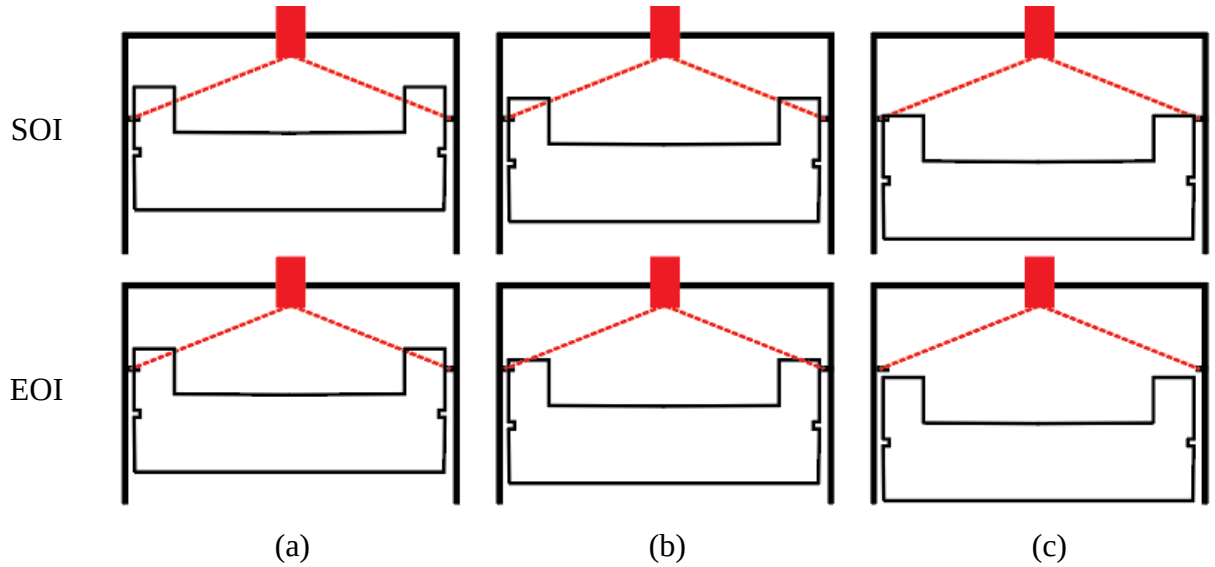


Figure 8: Spray axis orientation depicted (in dashed red) with respect to piston position for (a) Post SOI=15 CAD; (b) Post SOI=19 CAD and (c) Post SOI=25 CAD. Top row: Approximate piston position at SOI. Bottom row: Approximate piston position at the end of injection (EOI). Images not drawn to scale.

## 4. Conclusions

Preliminary results from an optical engine investigation of a triple-injection strategy employed for aftertreatment thermal management were presented. Three post injection times, 15, 19, and 25 CAD were the focus of this study. Schlieren and OH chemiluminescence imaging shed valuable insight into spray and combustion characteristics of the post injection. The following main conclusions were drawn:

- Pilot and Main Injection: Higher in-cylinder temperature and density at main SOI time ensures higher air entrainment and vaporization of the fuel jet. Heat release from these injections increases the in-cylinder temperature which helps maintain kinetically-relevant temperatures to ignite post injections introduced later in the expansion stroke.

- Post SOI 15: The high density and jet targeting result in fuel penetration that is predominantly limited to the piston bowl region. The high temperatures and density at SOI result in a short ignition delay.
- Post SOI 19 and 25: Lower ambient gas density during injection leads to lower entrainment of gases, which along with the reduced gas temperatures increases liquid fuel penetration. This combined with the jet targeting reduces the mass of fuel present in the piston bowl region. For the Post SOI 25 injection timing this results in lower soot concentration seen in the piston bowl region compared to the Post SOI 15 timing. It is not clear if overall concentrations are lower in-cylinder due to the limited field of view.
- Emissions trends from [23], suggests a general trend of increasing HC emissions as post injection is retarded further into expansion stroke. Liner impingement along with formation of over-lean pockets of fuel caused by overmixing, at late injection timing were identified as possible source of these emissions. The current jet imaging results provide additional support for these suggested mechanisms.

## 5. Acknowledgements

This material is based upon work supported by the U.S. Department of Energy's Office of Energy Efficiency and Renewable Energy (EERE) under the Bioenergy Technologies Office, Co-Optimization of Fuels & Engines initiative award number DE-EE0008480.

## 6. References

[1] US Energy Information Administration (EIA), Annual Energy Outlook 2020, 2020.
[2] M.S. Reiter, K.M. Kockelman, Transportation Research Part D: Transport and Environment. 43 (2016) 123–132. https://doi.org/10.1016/j.trd.2015.12.012.
[3] J.E. Dec, SAE Technical Papers. (1997). https://doi.org/10.4271/970873.
[4] D. Kim, J. Martz, A. Violi, Fuel. 180 (2016) 481–496. https://doi.org/10.1016/j.fuel.2016.03.085.
[5] R.N. Dahms, G.A. Paczko, S.A. Skeen, L.M. Pickett, Proceedings of the Combustion Institute. 36 (2017) 2615–2623. https://doi.org/10.1016/j.proci.2016.08.023.
[6] D.L. Siebers, SAE Technical Papers. (1998). https://doi.org/10.4271/980809.
[7] G. Guo, J. Warner, G. Cavataio, D. Dobson, E. Badillo, C. Lambert, SAE Technical Papers. (2010). https://doi.org/10.4271/2010-01-1183.
[8] C. Guardiola, B. Pla, P. Bares, J. Mora, International Journal of Engine Research. (2018). https://doi.org/10.1177/1468087418817965.
[9] M. Bouchez, J.B. Dementhon, SAE Technical Papers. 2000 (2000). https://doi.org/10.4271/2000-01-0472.
[10] A. Joshi, SAE Technical Papers. 2020-April (2020) 734–761. https://doi.org/10.4271/2020-01-0352.
[11] J.N. Chi, SAE Technical Papers. (2009). https://doi.org/10.4271/2009-01-0905.
[12] C.H. Kim, M. Paratore, E. Gonze, C. Solbrig, S. Smith, SAE Technical Papers. (2012) 2–11. https://doi.org/10.4271/2012-01-1092.
[13] U. Pfahl, A. Schatz, R. Konieczny, SAE Technical Papers. (2012). https://doi.org/10.4271/2012-01-1090.
[14] J. Parks, S. Huff, M. Kass, J. Storey, SAE Technical Papers. (2007). https://doi.org/10.4271/2007-01-3997.

[15] O. Salvat, P. Marez, G. Belot, SAE Technical Papers. 2000 (2000). https://doi.org/10.4271/2000-01-0473.
[16] J. O'Connor, M. Musculus, SAE International Journal of Engines. 6 (2013) 379–399. https://doi.org/10.4271/2013-01-0910.
[17] J. O'Connor, M. Musculus, SAE International Journal of Engines. 7 (2014) 673–693. https://doi.org/10.4271/2014-01-1255.
[18] Y. Hardalupas, C. Hong, C. Keramiotis, K.G. Ramaswamy, N. Soulopoulos, A.M.K.P. Taylor, D. Touloupis, G. Vourliotakis, M.A. Founti, International Journal of Engine Research. 18 (2017) 400–411. https://doi.org/10.1177/1468087416672511.
[19] C.L. Genzale, L.M. Pickett, S. Kook, SAE International Journal of Engines. 3 (2010) 479–495. https://doi.org/10.4271/2010-01-0610.
[20] A.T. Gaydon, The Spectroscopy of Flames, Chapman and Hall Ltd., 1974.
[21] M. Groendyk, D.A. Rothamer, Fuel. 252 (2019) 675–698. https://doi.org/10.1016/j.fuel.2019.03.094.
[22] N. Neal, D. Rothamer, Experiments in Fluids. 57 (2016). https://doi.org/10.1007/s00348-016-2239-0.
[23] T.W. Ross, N. Naser, S.L. Kokjohn, Inst. for Liq. Atomization and Spray Systems-Americas (2020), 2020.